Short Article

Structure

The Unusual Transmembrane Partition of the Hexameric Channel of the Hepatitis C Virus

Graphical Abstract

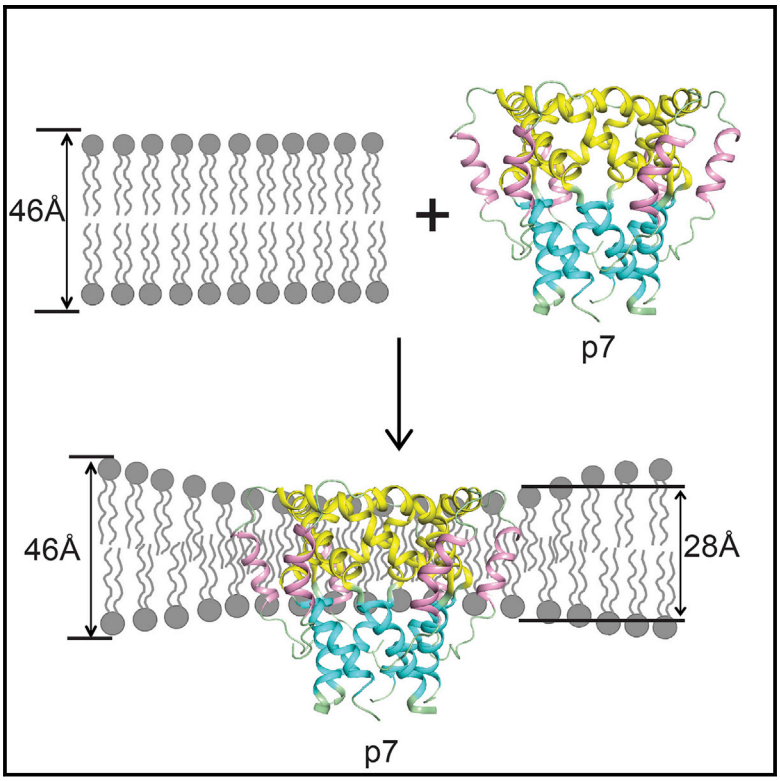

Authors

Wen Chen, Jyoti Dev, Julija Mezhyrova, Liqiang Pan, Alessandro Piai, James J. Chou

Correspondence

james_chou@hms.harvard.edu

In Brief

In this paper, Chen et al. observed unusual partition of the hexameric channel (p7) of hepatitis C virus in bicelles that mimic a lipid bilayer. Using methods such as OG-label, solvent/lipophilic PRE titration, and lipid NOE analysis, they found that p7 causes substantial thinning of its surrounding lipid bilayer.

Highlights

- NMR characterization of the HCV p7 channel in bicelles with q = 0.6
- p7 has similar secondary structure arrangement in detergent micelles and bicelles
- p7 forms hexamers in bicelles
- p7 partition in bicelles causes substantial thinning of the surrounding lipid bilayer

Chen et al., 2018, Structure *26*, 627–634
April 3, 2018 © 2018 Elsevier Ltd.
https://doi.org/10.1016/j.str.2018.02.011

CellPress

Structure
Short Article

The Unusual Transmembrane Partition of the Hexameric Channel of the Hepatitis C Virus

Wen Chen,[1,4] Jyoti Dev,[1,4] Julija Mezhyrova,[2] Liqiang Pan,[1] Alessandro Piai,[1] and James J. Chou[1,3,5,*]
[1]Department of Biological Chemistry and Molecular Pharmacology, Harvard Medical School, Boston, MA 02115, USA
[2]Institute of Biophysical Chemistry, Centre for Biomolecular Magnetic Resonance, J.W. Goethe-University, Frankfurt am Main, Germany
[3]State Key Laboratory of Molecular Biology, Shanghai Institute of Biochemistry and Cell Biology, Chinese Academy of Sciences, University of Chinese Academy of Sciences, Shanghai 201203, China
[4]These authors contributed equally
[5]Lead Contact
*Correspondence: james_chou@hms.harvard.edu
https://doi.org/10.1016/j.str.2018.02.011

SUMMARY

The p7 protein of the hepatitis C virus (HCV) can oligomerize in membrane to form cation channels. Previous studies showed that the channel assembly in detergent micelles adopts a unique flower-shaped oligomer, but the unusual architecture also presented problems for understanding how this viroporin resides in the membrane. Moreover, the oligomeric state of p7 remains controversial, as both hexamer and heptamer have been proposed. Here we address the above issues using p7 reconstituted in bicelles that mimic a lipid bilayer. We found, using a recently developed oligomer-labeling method, that p7 forms hexamers in the bicelles. Solvent paramagnetic relaxation enhancement analyses showed that the bilayer thickness around the HCV ion channel is substantially smaller than expected, and thus a significant portion of the previously assigned membrane-embedded region is solvent exposed. Our study provides an effective approach for characterizing the transmembrane partition of small ion channels in near lipid bilayer environment.

INTRODUCTION

The viroporin p7 encoded by the hepatitis C virus (HCV) genome is one of the better studied viral channels that has been validated as a target for developing drugs for treating HCV infections (Griffin et al., 2008; Steinmann et al., 2007). p7 is a small hydrophobic protein (63 amino acids) that can oligomerize in lipid bilayer to form cation-selective channels (Griffin et al., 2003; Pavlovic et al., 2003), with higher selectivity for Ca^{2+} than K^+/Na^+ (Montserret et al., 2010; Premkumar et al., 2004). The channel activity of p7 is important for the assembly and release of infectious viruses (Jones et al., 2007; Steinmann et al., 2007), and blocking p7-mediated ion conductance with inhibitors could substantially reduce virus production (Foster et al., 2011; Griffin et al., 2004; Mihm et al., 2006). In addition to the channel function, p7 has been shown to interact with the HCV nonstructural protein 2 (NS2), and this interaction is important for protein recruitment during virus assembly (Gouklani et al., 2013; Vieyres et al., 2013). Furthermore, the role of p7 and its interaction with NS2 have been implicated in capsid assembly and budding of the capsid into the ER (Boson et al., 2011; Gentzsch et al., 2013; Popescu et al., 2011).

As with many other viral membrane proteins, structural characterization of p7 was confronted with challenges of coping with the hydrophobic and dynamic nature of the protein. Earlier nuclear magnetic resonance (NMR) studies of p7 under conditions that support the monomeric state of the protein showed that p7 has three transmembrane (TM) helical segments: two in the N-terminal half of the sequence and one near the C terminus (Cook and Opella, 2011; Montserret et al., 2010). Although the monomeric state is unlikely to conduct ions, it could be involved in interacting with the NS2 protein during virus assembly (Gouklani et al., 2013; Vieyres et al., 2013). The oligomeric form of p7 was first examined using single-particle electron microscopy (EM), which showed that p7 from HCV genotype 2a (JFH-1 strain) assembles into hexamers in 1,2-diheptanoyl-*sn*-glycero-3-phosphocholine (DH^7PC) micelles, and the complex adopts a flower-like shape that does not resemble any of the known ion channel structures in the database (Luik et al., 2009). Later, a more detailed structure of the p7 hexamer was determined by solution NMR using p7 from genotype 5a (EUH1480 strain) reconstituted in dodecylphosphocholine (DPC) micelles (OuYang et al., 2013). Consistent with the flower-shaped EM images, the NMR structure shows a funnel-like architecture with six minimalist chains, each containing three TM helical segments: H1, H2, and H3. The H1 and H2 form the narrow and wide regions of the funnel-shaped cavity, respectively, and the H3 helices wrap the channel periphery by interacting with H1 and H2 (Figure S1A).

While the hexamer structure in detergent micelles suggested a channel architecture to permeate cations that is substantially different from any of the known K^+, Na^+, or Ca^{2+} channels, it also showed features that remain difficult to explain in the context of a membrane environment. The channel spans 45 Å along the symmetry axis, which would fit nicely in a lipid bilayer (~46 Å in thickness [Kucerka et al., 2011; Wiener and White, 1992]) (Figure S1B). However, such membrane partition of p7 would place two charged residues of H3, R54 and R57, deep in the hydrophobic core of the lipid bilayer, which translates to

12 lipid-facing charges in the context of the hexamer. This unusual feature raised concerns of possible structural artifacts caused by the detergent. Apart from the issue with membrane partition, the oligomeric state of p7 remains controversial, as heptameric assembly of p7 has also been proposed (Foster et al., 2014; Wang et al., 2014). Lessons from previous studies of viral membrane proteins suggest that these proteins are usually dynamic and are thus sensitive to membrane mimetics (Hong et al., 2012; Mei et al., 2012; OuYang and Chou, 2014; Zhou and Cross, 2013). The peculiar features reported for p7 could result from the different reconstitution media used for solubilizing the protein.

In this study, we address these issues using a p7 oligomer sample in bicelles that are sufficiently large ($q > 0.5$) to mimic a lipid bilayer (Glover et al., 2001; Lau et al., 2009; Sanders and Schwonek, 1992). We developed an oligomer-labeling technique (OG-label) to investigate p7 multimerization in the bicelles and found that p7 also assembles to hexamers in the more membrane-like environment. The bicelle sample is NMR feasible, which allowed comprehensive measurements of NMR secondary chemical shifts and relaxation parameters, as well as characterization of protein partition in the bicelles by solvent paramagnetic relaxation enhancement (PRE) analysis. Our NMR results collectively indicate that, unlike the previously proposed position of p7 in the membrane (Chandler et al., 2012; Cook et al., 2013; Foster et al., 2014; Montserret et al., 2010; OuYang et al., 2013; Patargias et al., 2006), the p7 channel caused substantial thinning of its surrounding bilayer, and as a result most of the H1 helices are solvent exposed. More importantly, this mode of membrane partitioning places the aforementioned H3 arginines, which were thought to immerse deeply in the lipid bilayer, near the lipid-solvent interface, providing an explanation for how this unusual viroporin structure is accommodated in the membrane.

RESULTS

Secondary Structure Mapping of p7 in Bicelles

To establish a bicelle system for the p7 channel, we used the p7 from genotype 5a (EUH1480 strain) (designated p7(5a)), which is one of the less hydrophobic sequences among the p7 variants. The purified protein was first solubilized in guanidine HCl, 1,2-dimyristoyl-*sn*-glycero-3-phosphocholine (DMPC), and 1,2-dihexanoyl-*sn*-glycero-3-phosphocholine (DH^6PC), following by dialysis to completely remove the denaturant while maintaining the q value (or the molar ratio of DMPC to DH^6PC) above 0.5. In the final NMR sample, q was measured to be 0.55, at which the estimated diameter of the lipid bilayer region of the bicelle disc is ~49.2 Å according to the equation describing bicelle assembly (Glover et al., 2001; Sanders and Schwonek, 1992; Sanders et al., 1994) (Figure 1A). Therefore, the proteins are in the near lipid bilayer environment. We found that the NMR spectrum of the bicelle sample is significantly different from that of p7(5a) in DPC micelles (Figure 1B). The relatively large bicelle size caused fast coherence relaxation for many TM residues, e.g., the average rotational correlation time (τ_c) for residues K33 and L56 at 30°C is ~33 ns in bicelles compared with ~24 ns in micelles (Figures S2A and S2B), posing serious challenges to NMR triple-resonance experiments. Nonetheless, about 95% of the backbone HN, N, C′, and Cα resonances were assigned using a combination of TROSY (transverse relaxation optimized spectroscopy)-HNCA (amide proton-to-nitrogen-to-α-carbon correlation) and HN-HN nuclear Overhauser enhancement (NOE) experiments (STAR Methods).

The backbone chemical shifts were further analyzed using TALOS+ (Shen et al., 2009) to examine the secondary structures. The Cα secondary shifts of p7(5a) in bicelles overall correlate well with those of p7(5a) in DPC micelles (Figure 1C), indicating that p7(5a) in bicelles also consist of H1, H2, and H3 helical segments in arrangement similar to that of the structure in micelles. Notably, the Cα secondary shifts of H1 in bicelles are substantially smaller than the corresponding shifts in micelles, suggesting that this helical segment is less helical in the bicelle-reconstituted protein.

The Oligomeric State of p7(5a) in Bicelles

Despite the similarity in secondary structures, the large NMR spectral difference suggests the importance of reevaluating the oligomeric state in bicelles. This task, however, posed serious technical challenges, as the p7(5a) oligomer does not survive the denaturing condition of SDS-PAGE (Figure S3A). Direct chemical crosslinking of p7(5a) using Lomant's reagents was inefficient and generated non-specific ladder patterns at higher crosslinker concentrations (Figure S3A), probably because the protein is mostly buried in bicelles and/or its primary amine groups are not well positioned for crosslinking. We thus developed an approach that circumvents the aforestated problems by first labeling, non-covalently, each of the protomers in the oligomer with a small soluble protein and then crosslinking the soluble protein to readout the oligomeric state. In this method, named OG-label and schematically illustrated in Figure 2A, the soluble crosslinkable protein (SCP) used is a small immunoglobulin-fold protein named GB1 (molecular weight 8.4 kDa), and its N terminus is linked to a TriNTA molecule via a PEG-2-SMCC (succinimidyl 4-(N-maleimidomethyl)cyclohexane-1-carboxylate) to form the TriNTA-GB1 conjugate (Figure S3B). The membrane protein to be examined has a His_6-tag. TriNTA has high binding affinity to His_6-tag (20 ± 10 nM) (Lata et al., 2005), which can strongly attach GB1 to the individual protomers of the membrane protein oligomer in bicelles. Thus, the concentration of stoichiometric amount of GB1 to the membrane protein oligomer allows for more efficient crosslinking than the free GB1 in solution. The crosslinked GB1 can be released from the oligomer by addition of EDTA and analyzed by SDS-PAGE.

To apply this method to the p7 oligomer, we prepared p7(5a) with N-terminal His_6-tag reconstituted in DMPC/DHPC bicelles (q = 0.6). Since p7 is expected to form high-order oligomers (≥6), a combination of the specific linker 3,3′-dithiobis(sulfosuccinimidyl propionate) (DTSSP) and the less specific linker glutaraldehyde was used to ensure that crosslinking of high-order oligomers is not limited by physical hindrance. We found that in the absence of p7(5a), treating 30 μM TriNTA-GB1 first with 0.6 mM DTSSP and then with 0.5 mM glutaraldehyde, gave rise to a dimer band in SDS-PAGE (Figure 2B). In the presence of 20 μM bicelle-reconstituted p7(5a), however, trimer, tetramer, and hexamer bands were also observed, and the hexamer band became stronger with higher glutaraldehyde concentration

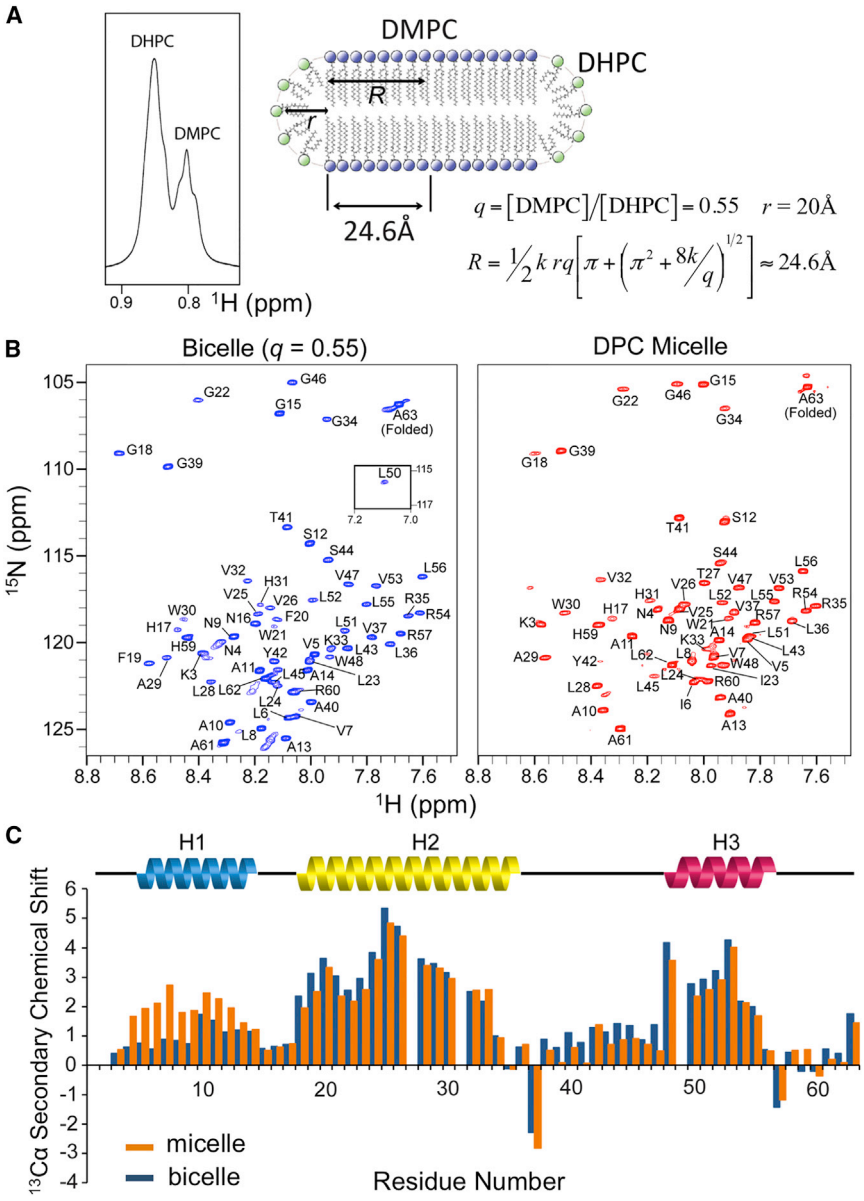

Figure 1. Comparison between p7(5a) in Bicelles and in Micelles

(A) Schematic illustration of an ideal DMPC/DHPC bicelle. The molar ratio of DMPC to DHPC (q) of the bicelle sample was determined by 1D NMR (left panel) to be 0.55. R and r are the radii of the planar region and the rim, respectively. The equation on the right (bottom) describes R as a function of q, where r = 20 Å and k = 0.6 is the ratio of head group density of DMPC to that of DHPC (Glover et al., 2001; Wu et al., 2010). When q = 0.55, R = 24.6 Å.

(B) The ^{1}H-^{15}N TROSY-HSQC spectra of p7(5a) in bicelle (left) and in DPC micelle (right). In both samples, the p7(5a) is (^{15}N, 85% ^{2}H) labeled.

(C) Comparison between the ^{13}Cα secondary chemical shifts of p7(5a) in bicelles (blue) and in DPC micelles (orange). The secondary shift values were calculated using TALOS+ (Shen et al., 2009). The chemical shift values of p7(5a) in DPC micelles were previously deposited (BMRB: 25685). The helical regions H1, H2, and H3 are defined according to the published NMR structure (PDB: 2M6X).

(Figure 2B). No heptamer band was visible. The results indicate that p7(5a) forms a hexamer in the bicelle.

Transmembrane Partition of p7(5a) in Bicelles

A previous study demonstrated that when bicelles are sufficiently large (q > 0.5), solvent PRE measurements are very effective for characterizing transmembrane partitioning of symmetric oligomers (Piai et al., 2017). This approach is based on the notion that if the bicelle is sufficiently wide, the lateral solvent PRE becomes negligible, thus allowing the use of measurable solvent PRE to probe residue-specific depth immersion of the protein along the bicelle normal axis. We thus performed the same analysis following the protocol in Piai et al. (2017), using p7(5a) reconstituted in bicelles with q = 0.6 (Figure S4B).

The water-soluble and membrane-inaccessible paramagnetic agent, Gd-DOTA (gadolinium(III) 1,4,7,10-tetraazacyclododecane-1,4,7,10-tetraacetate), was used to generate the solvent PRE. Gd-DOTA was titrated into the p7(5a) sample with [Gd-DOTA]/[p7(5a)] ratio ranging from 0.5 to 32. At each titration point, a 2D TROSY-HSQC (heteronuclear single-quantum coherence) spectrum was recorded to measure residue-specific PRE, defined here as the ratio of peak intensity in the presence (I) and absence (I_0) of the paramagnetic agent. For each of the residues, the PRE titration curve was fitted to exponential decay to derive the residue-specific PRE amplitude (PRE_{amp}) (Figures S4A and S4B; Table S1). The plot of PRE_{amp} versus (residue number) (Figure 3A) showed, unexpectedly, that H1 is mostly exposed as the PRE_{amp} value for this helical segment is essentially flat at ~0.9. Aside from H1, the rest of the protein including H2, H3, and connecting loops clearly span the bilayer twice, generating the "W"-shaped PRE profile. Notably, the PRE-sensitive regions of Figure 3A show remarkable correlation between the slope of PRE_{amp} versus (residue number) and protein main-chain orientation for various structured segments. For example, the rapid decrease of PRE_{amp} in residues 16–19 agrees with the steep angle (~63°) of this segment relative to the bilayer plane. The slow increase in residues 22–31 is consistent with the shallow angle (~33°) of the H2 helix in the bilayer. The H3 helix has a steep angle (~67°), which also agrees with the rapid increase of PRE_{amp} in residues 51–57. These close agreements suggest that the structure of the p7(5a) hexamer in bicelles is similar to the published NMR structure (OuYang et al., 2013).

To determine the position of the p7(5a) hexamer relative to the bilayer center, we calculated, for each residue i, the distance

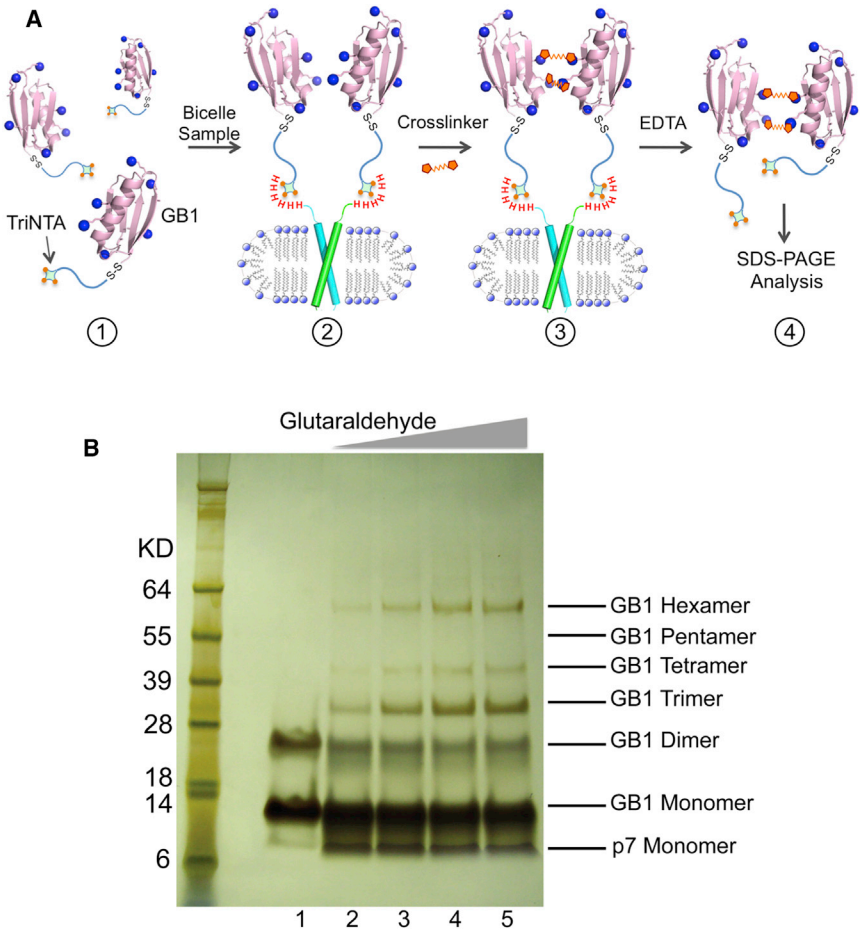

Figure 2. The Oligomer-Labeling Method for Determining the Oligomeric State of p7(5a) in Bicelles

(A) Schematic illustration of the oligomer-labeling (OG-label) method for characterizing the oligomeric state of transmembrane proteins in bicelles or micelles. (1) TriNTA-GB1 is sufficiently dilute to minimize non-specific crosslinking. (2) In the presence of the transmembrane oligomers (with His_6-tag) in bicelles, TriNTA-GB1 is recruited to the transmembrane oligomer in stoichiometric amount via strong affinity between His_6-tag and TriNTA. In this step, the primary amines of the membrane proteins are blocked prior to mixing with the TriNTA-GB1. (3) Addition of crosslinkers (first DTSSP and then glutaraldehyde) to crosslink the GB1s. (4) TriNTA-GB1 is released from the membrane protein by stripping off Ni^{2+} with EDTA, followed by SDS-PAGE analysis.

(B) SDS-PAGE analysis after the OG-label application to p7(5a) reconstituted in DMPC/DHPC bicelles with $q = 0.6$. For the control, 30 μM TriNTA-GB1 was treated first with 0.6 mM DTSSP and then with 0.5 mM of glutaraldehyde for 5 min (lane 1). In the presence of 20 μM bicelle-reconstituted p7(5a), 30 μM TriNTA-GB1 was treated first with 0.6 mM DTSSP and then with increasing amount of glutaraldehyde for 5 min: 0.1 mM (lane 2), 0.5 mM (lane 3), 1 mM (lane 4), and 2.5 mM (lane 5). The gel used for the SDS-PAGE was a 4%–12% Bis-Tris protein gel (Thermo Fisher Scientific).

along the protein symmetry axis (r_z), which is parallel to the bilayer normal, from the amide proton to an arbitrary reference point using the p7(5a) hexamer structure. This calculation converted PRE_{amp} versus (residue number) to PRE_{amp} versus r_z, which was then analyzed using the sigmoidal fitting method (Piai et al., 2017) (Figure S4C) to position the hexamer structure relative to the bilayer center (Figure 3C). The result shows that H2 and H3 are indeed TM helices buried in the lipid bilayer, with residues V26 of H2 and L51 of H3 approximately aligned with the bilayer center. The sigmoidal fit in Figure 3C shows that the PRE_{amp} reaches the maximum value at ~14 Å away from the bilayer center on either side, indicating that the bilayer thickness around the p7(5a) channel is ~28 Å. This bilayer thickness is substantially smaller than the 46 Å predicted for a DMPC bilayer, leaving most of the H1 helices exposed to the solvent (Figure 3D). The newly characterized membrane partition of p7(5a) also places R54, R57, and R60 of H3 as well as H17 at the end of the H1 at the edge of the bilayer (Figure 3D), as opposed to the middle of the bilayer (Figure S1B).

Complementary to the solvent PRE data, a set of lipophilic PRE data was also acquired. The bicelle-reconstituted ($q = 0.6$) p7(5a) was titrated with the membrane-embedded paramagnetic agent 16-doxyl-stearic acid (16-DSA) at various known concentrations, and the residue-specific PRE_{amp} was determined using the same approach as that employed for the solvent PRE (Figure 3E). We note that the dynamic range of PRE_{amp} of the lipophilic agent is significantly less than that of the solvent PRE_{amp} because (1) most of the structured regions of the protein are immersed in the bicelles and (2) the reduced thickness of the bicelle is expected to result in wider distribution of the terminal paramagnetic center of the 16-DSA within the bicelle; that is, the terminal nitroxide moieties are no longer localized at the center of the bilayer region of the bicelles. Nevertheless, the PRE_{amp} shows an overall "M"-shaped profile reciprocal to that of the solvent PRE_{amp}. The data show that the helical segments H2, H3, and connecting loops span the bilayer twice. Moreover, consistent with the solvent PRE data, the lower PRE_{amp} values of H1 than those of H2 and H3 indicate that the H1 helix is largely outside of the bilayer and solvent exposed.

In addition to the PRE analyses, we measured protein-lipid NOEs to further examine the transmembrane partition of p7(5a) in bicelles. We recorded a ^{15}N-edited NOE spectroscopy spectrum using a sample in which p7(5a) is [^{15}N,^{2}H] labeled and the bicelles ($q = 0.6$) are composed of regular DMPC and deuterated DH^6PC. The NOE strip plot (Figure S4D) shows that H1 has only water cross-peaks (from either NOE or exchange or both) and no lipid NOEs, indicating that it is solvent exposed and not partitioned in the lipid bilayer. For H2, which is the pore-forming helix, only a few lipid-exposed residues such as V26 and W30 show NOE to the DMPC acyl chain, and V37 at the wide opening of the channel shows water NOE. Most of the H2 residues show neither lipid nor water NOEs. Finally, H3, which is the lipid-facing

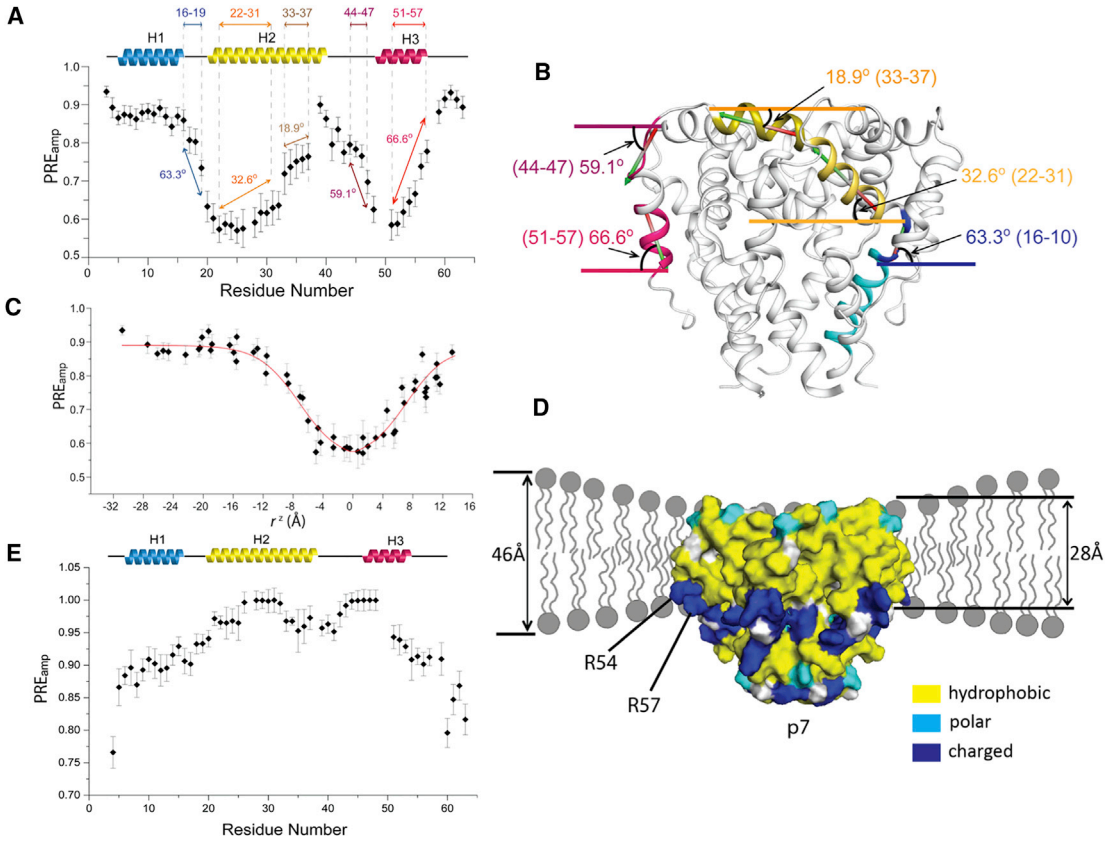

Figure 3. Membrane Partition of p7(5a) in Bicelles

(A) Residue-specific PRE amplitude (PRE_{amp}) of p7(5a) in bicelles with q = 0.6. The arrows (in different colors) indicate the fragments of the p7(5a) structure for which the slope of PRE_{amp} correlates well with the steepness of the fragment in the hexamer structure. The steepness is reported as the angle of the fragment relative to the bilayer plane (calculated using the PyMOL program [PyMOL Molecular Graphics System, Version 2.0; Schrödinger]).

(B) A side view of the p7(5a) structure showing the orientation of the fragments in (A) relative to the bilayer plane.

(C) The optimized fit of the PRE_{amp} versus r_z data to the symmetric sigmoidal function. The estimated thickness of the DMPC bilayer around p7 is about 28 Å.

(D) p7(5a) hexamer (in surface representation) causes substantial thinning of its surrounding bilayer. Hydrophobic, polar, and charged residues are shown in yellow, cyan, and blue, respectively.

(E) Residue-specific PRE_{amp} of p7(5a) determined from the lipophilic PRE analysis. PRE_{amp} was derived from 16-DSA titration. The "M" shape PRE_{amp} profile is reciprocal to the "W" shape profile of Gd-DOTA PRE_{amp} in (A), confirming that p7(5a) spans the bilayer twice, as well as the exposure of most of the H1 helices to solvent.

All error bars were calculated by the Origin software during function fitting.

helix, shows the strongest NOEs to the lipid. The NOE results were also mapped onto the structural model obtained in detergent micelles (Figure 4) and showed overall agreement with the PRE analyses.

DISCUSSION

We have characterized the oligomeric state and membrane partition of p7(5a) using a DMPC/DH^6PC bicelle system that closely mimics the lipid bilayer environment. Previous studies have shown that when $q > 0.5$, the DMPC/DH^6PC assembly reaches the ideal bicelle condition in which the lipid and detergents are well segregated (Glover et al., 2001; Piai et al., 2017). Our NMR and OG-label results were all obtained in bicelles with q values between 0.5 and 0.6, and thus should reflect the intrinsic properties of p7(5a) in a lipid bilayer. The results strongly indicate that the channel formed by p7(5a) is hexameric and shows a rather unusual membrane partition in which a significant portion of the channel is exposed to the solvent.

In the OG-label analysis, the SCP (TriNTA-GB1) was crosslinked to trimers, tetramers, and hexamers when attached to the bicelle-reconstituted p7(5a) (Figure 2B). This distribution in SDS-PAGE, however, should not reflect p7(5a) oligomerization in bicelles because such heterogeneity would have made the NMR resonances broad and not analyzable. We believe the presence of the different crosslinked species was due to the crosslinking properties of the SCP, e.g., linkage of dimer in a particular configuration may greatly reduce the probability of higher-order crosslinking. The fact that the hexamer band became stronger with higher crosslinker concentration (Figure 2B) is a strong indication that the number of SCPs attached to a p7(5a)-bicelle complex that were close enough to be crosslinked was 6. This number is consistent with the hexameric assemblies of p7(2a) in DH^7PC micelles (Luik et al., 2009) and

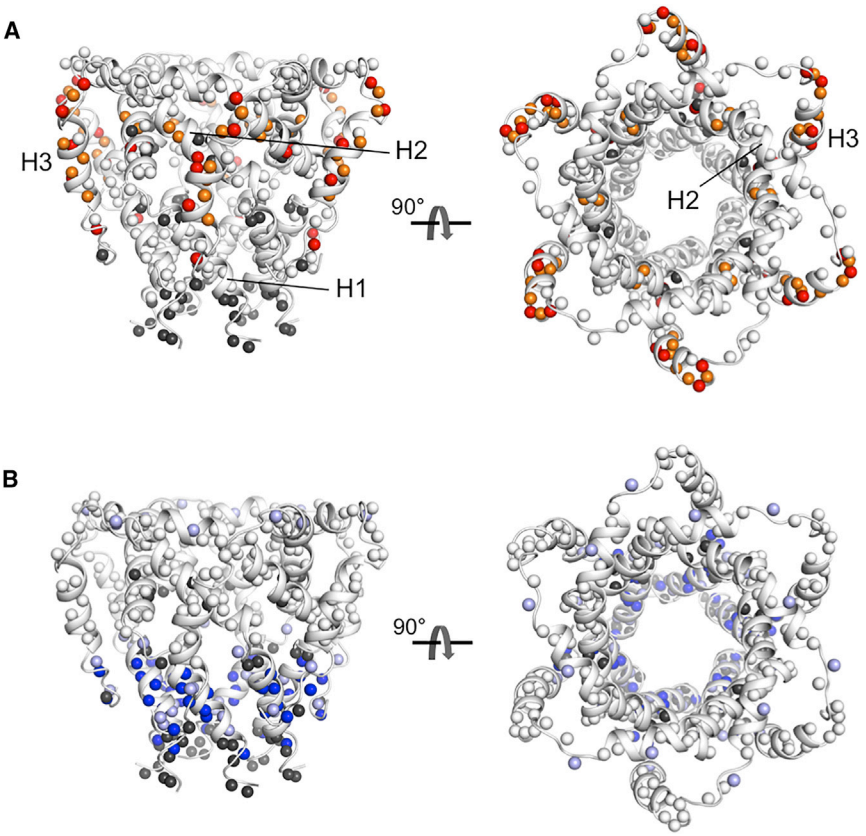

Figure 4. Mapping the Lipid NOEs from Bicelles onto the Structural Model of the p7(5a) Hexamer Obtained in Micelles

(A) The amide protons that show strong or weak lipid NOE are shown as red and orange spheres, respectively.

(B) The amide protons that show strong or weak water cross-peak are shown as blue and light blue, respectively.

In (A) and (B), the gray spheres indicate amide protons that do not show either lipid or water cross-peaks, while the black spheres indicate residues that could not be analyzed due to weak or overlapped resonances.

p7(5a) in DPC micelles (OuYang et al., 2013) observed by negative-stain EM. The agreement among the different genotypes of p7 in different membrane mimetic media implies that the intrinsic oligomeric state of p7 in the membrane is hexamer.

We emphasize that the OG-label method was critical for the oligomer characterization for the bicelle-reconstituted p7(5a). Since the bicelle is a dynamic assembly of lipid and detergent, it is extremely difficult to maintain the bicelle *q* in any size-exclusion-based analysis, e.g., size-exclusion chromatography with multi-angle light scattering. The equilibrium sedimentation method has been used before to investigate membrane protein size in detergent micelles, exemplified by the studies on the transmembrane domains (TMDs) of the glycophorin A and amyloid precursor proteins (Chen et al., 2014; Fleming et al., 2004) as well as the simian immunodeficiency virus envelope protein (Center et al., 2001). This method, however, requires very precise matching of solvent density to that of membrane mimetic media (Fleming, 2000), and this is also very difficult to achieve for bicelles. Furthermore, direct chemical crosslinking of hydrophobic, membrane-embedded proteins is difficult and often case dependent. The OG-label method thus provides a general solution to investigate the oligomeric state of small TM proteins in any media, including micelles, bicelles, nanodiscs, etc. While the use of GB1 as SCP in the OG-label analysis of p7(5a) produced acceptable results, we believe it is possible to find SCPs for achieving better crosslinking efficiency. Several considerations for the improvement include (1) good exposure and distribution of lysines for crosslinking, (2) good stability in detergent, and (3) sufficiently small size suitable for regular SDS-PAGE.

Due to the slow tumbling of p7(5a) reconstituted in the bicelles, i.e., $\tau_c \sim$ 33 ns for residues in the core structured region, we could not perform full-scale structure determination using the conventional NMR protocol used earlier for the micelle sample (OuYang et al., 2013). Nonetheless, the NMR data we managed to collect for the bicelle sample suggest that the conformations in bicelle and micelle are similar overall. First, the Cα secondary shifts from the two samples correlate remarkably well except for the H1 helix (Figure 1C), which showed substantially smaller secondary shifts in bicelles than in micelles. The smaller secondary shifts suggest that H1 is less helical in bicelles. This is consistent with the membrane partition of p7(5a) that H1 is mostly solvent exposed and possibly less well packed. Since detergent molecules do not form a bilayer, the entire p7(5a) channel was probably protected artificially by the micelle, providing interactions that made H1 more helical. Compared with H2 and H3, H1 is less structured in both bicelle and micelle, and this is consistent with the substantially smaller τ_c of residues in H1 than in H2 and H3 (Figure S2B). In the previous study of p7(5a) in micelles (OuYang et al., 2013), our structural interpretation led to the proposal that N9 of the H1 helix forms the cation binding filter. Our new results in bicelles suggest that, by virtual of being exposed and dynamic, residues of H1 should not play a key role in cation selectivity. The membrane partition information should provide guidance to searching for the major cation binding site in the channel.

Finally, our solvent PRE analysis of p7(5a) in bicelles indicates that the bilayer thickness around the channel is ~28 Å, which is substantially smaller than the 46 Å predicted for a DMPC bilayer. This thickness is barely sufficient to embed most of the H2 and H3 helices, leaving H1 exposed to the solvent (Figure 3D). This mode of membrane partition, although unusual, places the questionable arginines of H3 (R54 and R57) at the lipid-solvent interface, and is thus energetically favorable. Incidentally, in a similar solvent PRE analysis performed on the trimeric TMD of Fas, a death receptor of the tumor necrosis factor receptor superfamily, the bilayer thickness around the protein was found to be ~34 Å (Piai et al., 2017).

The apparent difference suggests an intriguing phenomenon that protein partition in membrane can modulate the lipid bilayer thickness around the proteins, and this effect likely depends on the nature of protein-lipid interactions.

In conclusion, the successful reconstitution of the p7(5a) channel in ideal bicelles (bicelles with $q > 0.5$) enabled us to obtain an accurate view of the membrane partition of the channel that is very different from what has been proposed based on the structure in micelles. At first, it was not clear that the p7(5a) oligomer (42 kDa) incorporated in bicelles of such size (49.2 Å in diameter) is feasible at all for high-resolution NMR spectroscopy. Our data show that, although the large bicelle system posed serious technical problems for performing a full-scale NOE analysis, it can nevertheless generate sufficiently high-quality NMR data for a thorough characterization of the secondary structure, membrane partition, and dynamics of the channel complex in an essentially lipid bilayer environment. We thus believe that the combined use of ideal bicelles, solvent PRE, and OG-label, as well as customized NOE experiments for large macromolecular complexes, represents an effective option for structural characterization of membrane proteins in a near lipid bilayer environment.

STAR★METHODS

Detailed methods are provided in the online version of this paper and include the following:

- KEY RESOURCES TABLE
- CONTACT FOR REAGENT AND RESOURCE SHARING
- METHOD DETAILS
  - Sample Preparation
  - Reconstitution of p7(5a) in Bicelles
  - NMR Resonance Assignment
  - Lipid NOE Detection
  - NMR Dynamics Measurements
  - NMR Chemical Shift Analysis
  - GB1 Expression and Purification
  - TriNTA-GB1 Conjugation
  - OG-label
  - Solvent PRE Analysis of p7(5a) Membrane Partition
  - Lipophilic PRE Analysis

SUPPLEMENTAL INFORMATION

Supplemental Information includes five figures and one table and can be found with this article online at https://doi.org/10.1016/j.str.2018.02.011.

ACKNOWLEDGMENTS

We thank Qingshan Fu and Chan Cao for insightful discussions. This work was supported by a National Key R&D Program of China grant (2017YFA0504801) and a US NIH grant GM116898 to J.J.C.

AUTHOR CONTRIBUTIONS

W.C., J.D., and J.J.C. conceived the study; W.C. and J.D. developed the NMR system of p7(5a) in bicelles; W.C., J.M., L.P., and J.J.C. developed the OG-label method; W.C. and A.P. performed the membrane partition analyses; W.C. and J.J.C. wrote the paper; all authors contributed to editing of the paper.

DECLARATION OF INTERESTS

The authors declare no competing interests.

Received: December 7, 2017
Revised: January 24, 2018
Accepted: February 9, 2018
Published: March 15, 2018

REFERENCES

Bartels, C., Xia, T.H., Billeter, M., Guntert, P., and Wuthrich, K. (1995). The program XEASY for computer-supported NMR spectral analysis of biological macromolecules. J. Biomol. NMR *6*, 1–10.

Boson, B., Granio, O., Bartenschlager, R., and Cosset, F.L. (2011). A concerted action of hepatitis C virus p7 and nonstructural protein 2 regulates core localization at the endoplasmic reticulum and virus assembly. PLoS Pathog. *7*, e1002144.

Center, R.J., Schuck, P., Leapman, R.D., Arthur, L.O., Earl, P.L., Moss, B., and Lebowitz, J. (2001). Oligomeric structure of virion-associated and soluble forms of the simian immunodeficiency virus envelope protein in the prefusion activated conformation. Proc. Natl. Acad. Sci. USA *98*, 14877–14882.

Chandler, D.E., Penin, F., Schulten, K., and Chipot, C. (2012). The p7 protein of hepatitis C virus forms structurally plastic, minimalist ion channels. PLoS Comput. Biol. *8*, e1002702.

Chen, W., Gamache, E., Rosenman, D.J., Xie, J., Lopez, M.M., Li, Y.M., and Wang, C. (2014). Familial Alzheimer's mutations within APPTM increase Abeta42 production by enhancing accessibility of epsilon-cleavage site. Nat. Commun. *5*, 3037.

Cheng, Y., and Patel, D.J. (2004). An efficient system for small protein expression and refolding. Biochem. Biophys. Res. Commun. *317*, 401–405.

Cook, G.A., Dawson, L.A., Tian, Y., and Opella, S.J. (2013). Three-dimensional structure and interaction studies of hepatitis C virus p7 in 1,2-dihexanoyl-sn-glycero-3-phosphocholine by solution nuclear magnetic resonance. Biochemistry *52*, 5295–5303.

Cook, G.A., and Opella, S.J. (2011). Secondary structure, dynamics, and architecture of the p7 membrane protein from hepatitis C virus by NMR spectroscopy. Biochim. Biophys. Acta *1808*, 1448–1453.

Delaglio, F., Grzesiek, S., Vuister, G.W., Zhu, G., Pfeifer, J., and Bax, A. (1995). NMRPipe: a multidimensional spectral processing system based on UNIX pipes. J. Biomol. NMR *6*, 277–293.

Fleming, K.G. (2000). Probing stability of helical transmembrane proteins. Methods Enzymol. *323*, 63–77.

Fleming, K.G., Ren, C.C., Doura, A.K., Eisley, M.E., Kobus, F.J., and Stanley, A.M. (2004). Thermodynamics of glycophorin A transmembrane helix dimerization in C14 betaine micelles. Biophys. Chem. *108*, 43–49.

Foster, T.L., Thompson, G.S., Kalverda, A.P., Kankanala, J., Bentham, M., Wetherill, L.F., Thompson, J., Barker, A.M., Clarke, D., Noerenberg, M., et al. (2014). Structure-guided design affirms inhibitors of hepatitis C virus p7 as a viable class of antivirals targeting virion release. Hepatology *59*, 408–422.

Foster, T.L., Verow, M., Wozniak, A.L., Bentham, M.J., Thompson, J., Atkins, E., Weinman, S.A., Fishwick, C., Foster, R., Harris, M., et al. (2011). Resistance mutations define specific antiviral effects for inhibitors of the hepatitis C virus p7 ion channel. Hepatology *54*, 79–90.

Gentzsch, J., Brohm, C., Steinmann, E., Friesland, M., Menzel, N., Vieyres, G., Perin, P.M., Frentzen, A., Kaderali, L., and Pietschmann, T. (2013). Hepatitis c Virus p7 is critical for capsid assembly and envelopment. PLoS Pathog. *9*, e1003355.

Glover, K.J., Whiles, J.A., Wu, G., Yu, N., Deems, R., Struppe, J.O., Stark, R.E., Komives, E.A., and Vold, R.R. (2001). Structural evaluation of phospholipid bicelles for solution-state studies of membrane-associated biomolecules. Biophys. J. *81*, 2163–2171.

Gouklani, H., Beyer, C., Drummer, H., Gowans, E.J., Netter, H.J., and Haqshenas, G. (2013). Identification of specific regions in hepatitis C virus

core, NS2 and NS5A that genetically interact with p7 and co-ordinate infectious virus production. J. Viral Hepat. *20*, e66–71.

Griffin, S., Stgelais, C., Owsianka, A.M., Patel, A.H., Rowlands, D., and Harris, M. (2008). Genotype-dependent sensitivity of hepatitis C virus to inhibitors of the p7 ion channel. Hepatology *48*, 1779–1790.

Griffin, S.D., Beales, L.P., Clarke, D.S., Worsfold, O., Evans, S.D., Jaeger, J., Harris, M.P., and Rowlands, D.J. (2003). The p7 protein of hepatitis C virus forms an ion channel that is blocked by the antiviral drug, Amantadine. FEBS Lett. *535*, 34–38.

Griffin, S.D., Harvey, R., Clarke, D.S., Barclay, W.S., Harris, M., and Rowlands, D.J. (2004). A conserved basic loop in hepatitis C virus p7 protein is required for amantadine-sensitive ion channel activity in mammalian cells but is dispensable for localization to mitochondria. J. Gen. Virol. *85*, 451–461.

Hong, M., Zhang, Y., and Hu, F. (2012). Membrane protein structure and dynamics from NMR spectroscopy. Annu. Rev. Phys. Chem. *63*, 1–24.

Jones, C.T., Murray, C.L., Eastman, D.K., Tassello, J., and Rice, C.M. (2007). Hepatitis C virus p7 and NS2 proteins are essential for production of infectious virus. J. Virol. *81*, 8374–8383.

Kucerka, N., Nieh, M.P., and Katsaras, J. (2011). Fluid phase lipid areas and bilayer thicknesses of commonly used phosphatidylcholines as a function of temperature. Biochim. Biophys. Acta *1808*, 2761–2771.

Lata, S., Reichel, A., Brock, R., Tampe, R., and Piehler, J. (2005). High-affinity adaptors for switchable recognition of histidine-tagged proteins. J. Am. Chem. Soc. *127*, 10205–10215.

Lau, T.L., Kim, C., Ginsberg, M.H., and Ulmer, T.S. (2009). The structure of the integrin alphaIIbbeta3 transmembrane complex explains integrin transmembrane signalling. EMBO J. *28*, 1351–1361.

Lee, D., Hilty, C., Wider, G., and Wuthrich, K. (2006). Effective rotational correlation times of proteins from NMR relaxation interference. J. Magn. Reson. *178*, 72–76.

Luik, P., Chew, C., Aittoniemi, J., Chang, J., Wentworth, P., Jr., Dwek, R.A., Biggin, P.C., Venien-Bryan, C., and Zitzmann, N. (2009). The 3-dimensional structure of a hepatitis C virus p7 ion channel by electron microscopy. Proc. Natl. Acad. Sci. USA *106*, 12712–12716.

Mei, Z., Yan, P., Situ, B., Mou, Y., and Liu, P. (2012). Cryptotanshinione inhibits beta-amyloid aggregation and protects damage from beta-amyloid in SH-SY5Y cells. Neurochem. Res. *37*, 622–628.

Meier, S., Guthe, S., Kiefhaber, T., and Grzesiek, S. (2004). Foldon, the natural trimerization domain of T4 fibritin, dissociates into a monomeric A-state form containing a stable beta-hairpin: atomic details of trimer dissociation and local beta-hairpin stability from residual dipolar couplings. J. Mol. Biol. *344*, 1051–1069.

Mihm, U., Grigorian, N., Welsch, C., Herrmann, E., Kronenberger, B., Teuber, G., von Wagner, M., Hofmann, W.P., Albrecht, M., Lengauer, T., et al. (2006). Amino acid variations in hepatitis C virus p7 and sensitivity to antiviral combination therapy with amantadine in chronic hepatitis C. Antivir. Ther. *11*, 507–519.

Montserret, R., Saint, N., Vanbelle, C., Salvay, A.G., Simorre, J.P., Ebel, C., Sapay, N., Renisio, J.G., Bockmann, A., Steinmann, E., et al. (2010). NMR structure and ion channel activity of the p7 protein from hepatitis C virus. J. Biol. Chem. *285*, 31446–31461.

OuYang, B., and Chou, J.J. (2014). The minimalist architectures of viroporins and their therapeutic implications. Biochim. Biophys. Acta *1838*, 1058–1067.

OuYang, B., Xie, S., Berardi, M.J., Zhao, X., Dev, J., Yu, W., Sun, B., and Chou, J.J. (2013). Unusual architecture of the p7 channel from hepatitis C virus. Nature *498*, 521–525.

Patargias, G., Zitzmann, N., Dwek, R., and Fischer, W.B. (2006). Protein-protein interactions: modeling the hepatitis C virus ion channel p7. J. Med. Chem. *49*, 648–655.

Pavlovic, D., Neville, D.C., Argaud, O., Blumberg, B., Dwek, R.A., Fischer, W.B., and Zitzmann, N. (2003). The hepatitis C virus p7 protein forms an ion channel that is inhibited by long-alkyl-chain iminosugar derivatives. Proc. Natl. Acad. Sci. USA *100*, 6104–6108.

Piai, A., Fu, Q., Dev, J., and Chou, J.J. (2017). Optimal bicelle size q for solution NMR studies of the protein transmembrane partition. Chemistry *23*, 1361–1367.

Popescu, C.I., Callens, N., Trinel, D., Roingeard, P., Moradpour, D., Descamps, V., Duverlie, G., Penin, F., Héliot, L., Rouillé, Y., et al. (2011). NS2 protein of hepatitis C virus interacts with structural and non-structural proteins towards virus assembly. PLoS Pathog. *7*, e1001278.

Premkumar, A., Wilson, L., Ewart, G.D., and Gage, P.W. (2004). Cation-selective ion channels formed by p7 of hepatitis C virus are blocked by hexamethylene amiloride. FEBS Lett. *557*, 99–103.

Salzmann, M., Wider, G., Pervushin, K., and Wuthrich, K. (1999). Improved sensitivity and coherence selection for [^{15}N,^{1}H]-TROSY elements in triple resonance experiments. J. Biomol. NMR *15*, 181–184.

Sanders, C.R., 2nd, and Schwonek, J.P. (1992). Characterization of magnetically orientable bilayers in mixtures of dihexanoylphosphatidylcholine and dimyristoylphosphatidylcholine by solid-state NMR. Biochemistry *31*, 8898–8905.

Sanders, C.R., Hare, B.J., Howard, K.P., and Prestegard, J.H. (1994). Magnetically-oriented phospholipid micelles as a tool for the study of membrane-associated molecules. Prog. Nucl. Magn. Reson. Spectrosc. *26*, 421–444.

Shen, Y., Delaglio, F., Cornilescu, G., and Bax, A. (2009). TALOS+: a hybrid method for predicting protein backbone torsion angles from NMR chemical shifts. J. Biomol. NMR *44*, 213–223.

Spera, S., and Bax, A. (1991). An empirical correlation between protein backbone conformation and Ca and Cb chemical shifts. J. Am. Chem. Soc. *113*, 5490–5492.

Steinmann, E., Penin, F., Kallis, S., Patel, A.H., Bartenschlager, R., and Pietschmann, T. (2007). Hepatitis C virus p7 protein is crucial for assembly and release of infectious virions. PLoS Pathog. *3*, e103.

Vieyres, G., Brohm, C., Friesland, M., Gentzsch, J., Wolk, B., Roingeard, P., Steinmann, E., and Pietschmann, T. (2013). Subcellular localization and function of an epitope-tagged p7 viroporin in hepatitis C virus-producing cells. J. Virol. *87*, 1664–1678.

Vranken, W.F., Boucher, W., Stevens, T.J., Fogh, R.H., Pajon, A., Llinas, M., Ulrich, E.L., Markley, J.L., Ionides, J., and Laue, E.D. (2005). The CCPN data model for NMR spectroscopy: development of a software pipeline. Proteins *59*, 687–696.

Walsh, J.D., Meier, K., Ishima, R., and Gronenborn, A.M. (2010). NMR studies on domain diffusion and alignment in modular GB1 repeats. Biophys. J. *99*, 2636–2646.

Wang, Y.T., Schilling, R., Fink, R.H., and Fischer, W.B. (2014). Ion-dynamics in hepatitis C virus p7 helical transmembrane domains—a molecular dynamics simulation study. Biophys. Chem. *192*, 33–40.

Wiener, M.C., and White, S.H. (1992). Structure of a fluid dioleoylphosphatidylcholine bilayer determined by joint refinement of x-ray and neutron diffraction data. III. Complete structure. Biophys. J. *61*, 434–447.

Wishart, D.S., and Sykes, B.D. (1994). The ^{13}C chemical-shift index: a simple method for the identification of protein secondary structure using ^{13}C chemical-shift data. J. Biomol. NMR *4*, 171–180.

Wu, H., Su, K., Guan, X., Sublette, M.E., and Stark, R.E. (2010). Assessing the size, stability, and utility of isotropically tumbling bicelle systems for structural biology. Biochim. Biophys. Acta *1798*, 482–488.

Zhou, H.X., and Cross, T.A. (2013). Influences of membrane mimetic environments on membrane protein structures. Annu. Rev. Biophys. *42*, 361–392.

Zhou, P., Lugovskoy, A.A., and Wagner, G. (2001). A solubility-enhancement tag (SET) for NMR studies of poorly behaving proteins. J. Biomol. NMR *20*, 11–14.

STAR★METHODS

KEY RESOURCES TABLE

REAGENT or RESOURCE	SOURCE	IDENTIFIER
Bacterial and Virus Strains		
E. coli BL21(DE3)	New England Biolabs	Cat# C2527
E. coli DH5-alpha	New England Biolabs	Cat# C2987
Chemicals, Peptides, and Recombinant Proteins		
Cyanogen Bromide	Sigma	Cat# C91492
DMPC Lipid	Avanti Polar Lipids	Cat# 850345
DH^{6}PC Detergent	Avanti Polar Lipids	Cat# 850305
TriNTA	Medicilon Inc.	N/A
SMCC Crosslinker	Life Technology	Cat# 22103
Triethylammonium Acetate	Calbiochem	Cat# 625718
Gd-DOTA	Macrocyclics, Inc.	Cat# M-147
16-DSA	Sigma-Aldrich	Cat# 253596
Software and Algorithms		
Sparky	Goddard, UCSF	www.cgl.ucsf.edu/home/sparky
Nmrpipe	Delaglio et al., 1995	www.ibbr.umd.edu/nmrpipe
Ccpnmr	Vranken et al., 2005	http://www.ccpn.ac.uk
Origin	OriginLab	www.originlab.com
Pymol	Schrodinger, LLC	www.pymol.org
Talos+	Shen et al., 2009	www.ibbr.umd.edu/nmrpipe
Other		
Hispur Ni-NTA Resin	Thermo Fisher	Cat# 88223
Zorbax SB-C18 Column	Agilent	Cat# 880995-202
Centricon Concentrator	EMD Millipore	Cat# UFC901024
StrepTrap HP Column	GE Healthcare	Cat# 28907547
Superdex S75 26/60	GE Healthcare	Cat# 28989334
NHS-Activated Agrose Resin	Thermo Fisher	Cat# 26196

CONTACT FOR REAGENT AND RESOURCE SHARING

Further information and requests for resources and reagents should be directed to and will be fulfilled by the Lead Contact James Chou (james_chou@hms.harvard.edu)

METHOD DETAILS

Sample Preparation

The expression and purification of p7(5a) followed exactly a previously published protocol (OuYang et al., 2013). Briefly, the amino acid sequence of p7 from genotype 5a was slightly modified for better protein solubility and sample stability. Three cysteines at positions 2, 27, and 44 were replaced with Ala, Thr and Ser, respectively. In addition, T1 was replaced with Gly, and A12 was replaced with Ser. The p7(5a) was fused to the trpLE sequence with an N-terminal His_9-tag in pMM LR6 vector (gift from S.C. Blacklow, Harvard Medical School). p7(5a) was transformed into *E. Coli* BL21 cells. Cells were grown in M9 minimal media until OD_{600} reached 0.7, and then cooled to 25°C before induction with 150 μM isopropyl-β-d-thiogalactopyranoside (IPTG). Cells were harvested after overnight expression. Protein purification was performed at room temperature. Inclusion bodies were collected by centrifugation at 22,000 g after cell lysis by sonication. Inclusion bodies were then resuspended with buffer containing 6 M guanidine HCl, 50 mM Tris, 200 mM NaCl, 1% (vol/vol) Triton X-100 (pH 8.0). The trpLE-p7(5a) fusion protein in the suspension was bound to HisPur Ni-NTA resin (Life technology) (1ml/1L culture) for 30 min, followed by sequential washing with 8 M urea solution and water. The fusion protein was then eluted from Ni-NTA resin with 90% (vol/vol) formic acid. Cyanogen bromide (Sigma) (0.2 g/ml) was added to the

formic acid elution to release p7(5a) from trpLE fusion partners for 1 hour under nitrogen gas. The mixture was dialyzed to remove excessive cyanogen bromide and lyophilized. p7(5a) was then separated from the cleaved mixture through reverse-phase HPLC (RP-HPLC) on a gradient from 40% acetonitrile (0.1% (vol/vol) trifluoroacetic acid) to 60% acetonitrile (0.1% (vol/vol) trifluoroacetic acid), using a Zorbax SB-C18 semi-preparative column (Agilent). The HPLC purified p7(5a) was then lyophilized and validated by SDS-PAGE.

Reconstitution of p7(5a) in Bicelles

Around 2 mg of p7(5a) dry powder was dissolved with 12 mg of 1,2-Dimyristoyl-*sn*-Glycero-3-Phosphocholine (DMPC) (Avanti Polar Lipids) and 16 mg of 1,2-Dihexanoyl-*sn*-Glycero-3-Phosphocholine (DH^6PC) (Avanti Polar Lipids) in 500 μl of 6 M guanidine HCl. The mixture was dialyzed against NMR buffer (25 mM MES, 25 mM NaCl, pH 6.5) for three hours at low stirring speed (100 rpm), followed by an additional round of dialysis for three hours at fast stirring speed (800 rpm). During the secondary round of dialysis, 3 mg of DH^6PC was added to the sample after every hour to ensure that the bicelle $q < 1$. After dialysis, the sample was concentrated to ~300 μl using Centrcon concentrator (EMD Millipore; MWCO,10 kD). The q was reported by 1D NMR and adjusted accordingly to 0.5-0.6 by addition of DH^6PC. The final p7(5a) concentration was ~1 mM (monomer concentration), while DMPC concentration was ~60 mM.

NMR Resonance Assignment

All NMR experiments were conducted at 30°C on Bruker spectrometers equipped with cryogenic probes. NMR spectra were processed using NMRpipe (Delaglio et al., 1995) and analyzed using Sparky (T. D. Goddard and D. G. Kneller, SPARKY 3, University of California, San Francisco) and ccpNMR (Vranken et al., 2005). Sequence-specific assignment of backbone chemical shifts ($^1H^N$, ^{15}N, $^{13}C\alpha$, and $^{13}C'$) was accomplished using two pairs of TROSY-enhanced triple resonance experiments, including HNCA, HN(CO)CA, HN(CA)CO, and HNCO (Salzmann et al., 1999). In addition, a 3D ^{15}N-edited NOESY-TROSY-HSQC experiment (200 ms NOE mixing time) was performed to validate the assignment. These spectra were all recorded using a (^{15}N, ^{13}C, 85% ^2H)-labeled p7(5a) sample.

Lipid NOE Detection

For measuring protein-lipid contacts, (^{15}N, ^2H)-labeled p7(5a) was reconstituted in bicelles made of regular DMPC and deuterated DH^6PC (1,2-dihexanoyl-d22-*sn*-glycero-3-phosphocholine; Avanti Polar Lipids) (q = 0.6), as described above. A 3D ^{15}N-edited NOESY-TROSY-HSQC spectrum (160 ms NOE mixing) was recorded at 30°C on a 600 MHz Bruker spectrometer equipped with cryogenic probe. The NOE spectrum was analyzed using XEASY (Bartels et al., 1995).

NMR Dynamics Measurements

Residue-specific rotational correlation time (τ_c) was measured using a 2D version (implemented in our lab) of the 1D experiment known as TRACT (TROSY for rotational correlation times) (Lee et al., 2006). For this experiment, a sample of 1 mM (^{15}N, 85% ^2H)-labeled p7(5a) reconstituted in bicelles with q = 0.55 was used. In the TRACT experiment, ^{15}N relaxation delays were set to 8, 16, 20, 24, 32, 40, 80, 96 ms for the TROSY component, and set to 8, 16, 32, 40, 56 ms for anti-TROSY component. Due to the fast relaxation of the anti-TROSY component, 5-fold more scans were used for recording the anti-TROSY spectra. For each of the assigned peaks, the R_2 relaxation rate of the TROSY (R_2^{α}) and anti-TROSY (R_2^{β}) components were determined by fitting the measurements to the exponential decay function:

$$\frac{I}{I_0} = y + A * e^{-R*Delay}, \qquad \text{(Equation 1)}$$

where I and I_0 represent the peak intensity with and without relaxation delay, respectively. Data fitting was done using the Origin program (OriginLab, Northampton, MA). τ_c was derived from the following equations:

$$R_\beta - R_\alpha = 2p\delta_N\,(4J(0) + 3J(\omega_N))(3cos^2\theta - 1)$$

$$J(\omega) = 0.4\tau_c / [1 + (\tau_c\omega)^2], \qquad \text{(Equation 2)}$$

where p is the dipole-dipole coupling between ^1H and ^{15}N and δ_N is the chemical shift anisotropy of the ^{15}N nucleus with the parameter $\theta = 17°$, and ω is the spectrometer ^{15}N frequency (60 MHz).

NMR Chemical Shift Analysis

The assigned backbone chemical shift values (^{15}N, $^{13}C\alpha$, $^{13}C'$) from the bicelle-reconstituted p7(5a) were used as input for TALOS+ program (Shen et al., 2009) to predict backbone dihedral angles and to calculate secondary Cα shift. Out of 58 residues with assignments, the dihedral angles of 43 residues were considered as 'GOOD' by TALOS+. The same TALOS+ analysis was done using the previously deposited chemical shift values of p7(5a) in DPC (downloaded from the Biological Magnetic Resonance Data Bank; BMRB accession number 25685). In this case, 'GOOD' prediction was made for 48 out of 58 residues. The Cα secondary chemical shift is

strongly dependent on the secondary structure of the protein (Spera and Bax, 1991; Wishart and Sykes, 1994). The calculated secondary Cα shifts from the bicelle sample were directly compared with those from the DPC sample.

GB1 Expression and Purification

GB1 protein is the B1 domain of protein G (56 residues), often used as part of a fusion protein to keep other domains in solution due to its high solubility and stability (Cheng and Patel, 2004; Zhou et al., 2001). The GB1 we used for OG-label contains 6 surface exposed lysines. For chemical conjugation with TriNTA and for potential purification purposes, a sequence containing a N-terminal Cys and a Strep-tag (CKDKDKDKWSHPQFEK) was added to the N-terminus of the GB1 sequence (Figure S3B). In addition, Thr2 of the native sequence was mutated to Gln for higher purification yield (Walsh et al., 2010). The modified GB1 DNA was inserted into the pET15b vector (free of His-tag), and the plasmid was transformed to *E. Coli* BL21 cells. Protein expression was induced with 1 mM IPTG at 37°C when the cell culture OD_{600} reached 0.6. Cells were harvested after 4 hours of incubation, resuspended in buffer A (100 mM Tris, 150 mM NaCl, 1 mM EDTA, 5 mM DTT (pH 8)), and then lysed by sonication. Cell debris was removed by centrifugation at 22,000 g for 30 min and the supernatant was applied to the StrepTrap HP column (GE Healthcare), pre-equilibrated with buffer A. The pure GB1 was eluted using 2.5 mM desthiobiotin in buffer A. The eluent was further purified by size exclusion over a Superdex S75 26/60 column (GE Healthcare) in a 25 mM HEPES buffer(5 mM DTT, pH 7.2). Pure GB1 was stored at -80°C upon further use.

TriNTA-GB1 Conjugation

TriNTA with a free primary amine (Figure S3B) was synthesized by Medicilon Inc. (Shanghai, China) and stored as dry powder at -20°C. The bi-functional crosslinker PEG2-SMCC (succinimidyl 4-(N-maleimidomethyl)cyclohexane-1-carboxylate) was incubated with TriNTA in 100 mM sodium carbonate buffer (pH 8.0) at the molar ratio of 4:1 for 1 hour to achieve more than 95% reaction efficiency. The SMCC-linked TriNTA was then purified by RP-HPLC with a Zorbax SB-C18 semi-preparative column (Agilent) through a gradient of 5-20% acetonitrile containing 0.1 M Triethylammonium acetate (TEAA) (Calbiochem) as buffering reagent, followed by lyophilization. SMCC-TriNTA was lyophilized before reacting with the Cys-containing GB1 mutant. Before crosslinking the SMCC-linked TriNTA to the Cys-containing GB1 via the melaimide chemistry, DTT in the stored GB1 sample was first removed using a PD-10 column (GE Healthcare). The SMCC-TriNTA was added to the GB1 sample at 2:1 molar ratio in a HEPES buffer (pH 7.2). The reaction mixture was degassed for 30 min and incubated for additional 30 min to achieve close to 90% completion of the reaction (Figure S3B). Ni^{2+} was then added to TriNTA-GB1 conjugate at 3:1 molar ratio to charge the NTAs with Ni^{2+}. Finally, TriNTA-GB1 was purified using a His_6-tag column, made in the lab by chemically linking a His_6-tagged foldon protein to NHS-Activated Agrose resin (Thermo Fisher Scientific). Foldon is the C-terminal domain of T4 fibritin; it has 27 residues and forms highly-stable trimer under normal conditions (Meier et al., 2004). The Ni^{2+}-charged TriNTA-GB1 was loaded to the His_6-foldon resin and incubated for 30 min. The resin was washed with 5 column volumes of washing buffer containing 25 mM HEPES, 100 mM NaCl (pH 7.2), followed by elution with 200 mM imidazole in the washing buffer (Figure S3B). Pure Ni^{2+}-activated TriNTA-GB1 was dialyzed against 25 mM HEPES (pH7.2) buffer and stored at 4°C for OG-label experiments.

OG-label

For performing the OG-label experiment on the bicelle-reconstituted p7(5a), the protein was modified by an N-terminus addition of a His_6-tag. The His_6-tagged p7(5a) was expressed, purified, and reconstituted in bicelles ($q = 0.6$) in the same way as described above for other NMR samples except HEPES (pH 7.2) was used as buffer for better crosslinking efficiency. To prevent undesirable crosslinking between p7(5a) and GB1, we first blocked all the active amine groups with the addition of 100-fold molar excess of Sulfo-NHS Acetate (Thermo Fisher Scientific) to the bicelle sample in 25 mM HEPES buffer (pH 7.2) for 1 hour at room temperature. Excessive Sulfo-NHS Acetate was removed by dialysis while tightly controlling the bicelle q as described above. After dialysis, 20 μM of p7(5a) (monomer concentration) was mixed with 30 μM TriNTA-GB1 to ensure the His_6-tagged p7(5a) are saturated with TriNTA-GB1. The mixture was then treated with 0.6 mM of DTSSP for 30 min, followed by incubation with various concentration (0.1, 0.5, 1.0, and 2.5 mM) of glutaraldehyde for 5 min. The crosslinking reaction was quenched with a 20 mM Tris buffer (pH 7.5). As a negative control, 0.6 mM of DTSSP and 0.5 mM of glutaraldehyde were sequentially added to 30 μM TriNTA-GB1 in the absence of the His_6-tagged p7(5a). The crosslinked species were examined by SDS-PAGE using the 4-12% Bis-Tris protein gels (Thermo Fisher Scientific).

Solvent PRE Analysis of p7(5a) Membrane Partition

We previously developed a solvent PRE method to determine the protein transmembrane partition in bicelles(Piai et al., 2017). DMPC/DH^6PC bicelle with sufficiently large q (> 0.5) allows direct use of measurable solvent PRE to probe residue-specific depth immersion of the protein in the bilayer region of the bicelle (Figure S4A). The solvent PRE measurements were thus performed using a 1 mM (^{15}N, 85% ^{2}H)-labeled p7(5a) reconstituted in bicelles with $q = 0.6$. The water-soluble and membrane inaccessible paramagnetic agent, Gd-DOTA (Macrocyclics, Inc.) was titrated into the bicelle sample to different concentrations indlucing 0, 0.5, 1, 1.5, 2, 4, 6, 8, 12, 16, and 32 mM. At each titration point, a 2D ^{15}N TROSY-HSQC spectrum was recorded using a 600 MHz Bruker spectrometer equipped with a cryogenic probe. The recovery delay was set to 3.5 seconds. The residue-specific PRE is defined as the ratio of peak intensity in the presence (I) and absence (I_0) of the paramagnetic agent. Peak intensities were measured at peak local maxima using quadratic interpolation to identify peak centers. For individual peaks, Origin was used to fit I/I_0 vs. Gd-DOTA concentration to the exponential decay

$$\frac{I}{I_0} = 1 - \mathrm{PRE}_{\mathrm{amp}}\left(1 - e^{-[\mathrm{Gd-DOTA}]/\tau}\right) \quad \text{(Equation 3)}$$

to derive the residue-specific PRE amplitude ($\mathrm{PRE}_{\mathrm{amp}}$) (Figure S4B).

To determine the position of the p7(5a) relative to the bilayer center, we calculated, for each residue *i*, the distance (r_z) along the protein symmetry axis, from the amide proton to an arbitrary choice of reference point based on the NMR structure of p7(5a). As such, the $\mathrm{PRE}_{\mathrm{amp}}$ vs (residue number) plot was converted to $\mathrm{PRE}_{\mathrm{amp}}$ vs r_z, which was then analyzed using the sigmoidal fitting method (details can be found in (Piai et al., 2017)). Briefly, the p7(5a) structure was moved along the 6-fold axis in increment of 0.5 Å and 0.1 Å (when approaching the true center) (Figure S4C) to achieve the best fit to the symmetric sigmoid equation

$$\mathrm{PRE}_{\mathrm{amp}} = \mathrm{PRE}^{\mathrm{min}}_{\mathrm{amp}} + \frac{\left(\mathrm{PRE}^{\mathrm{max}}_{\mathrm{amp}} - \mathrm{PRE}^{\mathrm{min}}_{\mathrm{amp}}\right)}{1 + e^{\left(\left(r^{I}_{z} - |r_z|\right)/\mathrm{SLOPE}\right)}} \quad \text{(Equation 4)}$$

where $\mathrm{PRE}^{\mathrm{min}}_{\mathrm{amp}}$ and $\mathrm{PRE}^{\mathrm{max}}_{\mathrm{amp}}$ are the limits within which $\mathrm{PRE}_{\mathrm{amp}}$ can vary for a particular protein system, r^{I}_{z} is the inflection point (the distance from the bilayer center at which $\mathrm{PRE}_{\mathrm{amp}}$ is halfway between $\mathrm{PRE}^{\mathrm{min}}_{\mathrm{amp}}$ and $\mathrm{PRE}^{\mathrm{max}}_{\mathrm{amp}}$), and SLOPE is a parameter which reports the steepness of the curve at the inflection point. A series of $\mathrm{PRE}_{\mathrm{amp}}$ vs r_z were calculated for different positions of the hexamer along the bilayer normal and fitted against Equation 4. The best fit (Figure S4C) gave an adjusted coefficient of determination (R^2_{adj}) of 0.908, and was used to determine the position of the hexamer structure with respect to the bilayer center $(r_z = 0)$.

Lipophilic PRE Analysis

The lipophilic PRE measurements were performed using a 1 mM (^{15}N, 85% ^{2}H)-labeled p7(5a) reconstituted in bicelles with $q = 0.6$. A stock solution of lipophilic paramagnetic agent 16-DSA (Sigma-Aldrich) was prepared at 24 mM concentration in the same buffer as that of the p7(5a) sample to prevent changes in the bicelle q value upon addition of the titrant. The progress of the titration was monitored by measuring 2D TROSY-HSQC spectrum at each of the following 16-DSA concentrations: 0, 0.25, 0.5, 1, 1.5, 2, 4, and 8 mM. The residue-specific $\mathrm{PRE}_{\mathrm{amp}}$ was determined by fitting the peak intensity decay as a function of [16-DSA] to Equation 3.

Structure, Volume *26*

Supplemental Information

The Unusual Transmembrane Partition of the Hexameric Channel of the Hepatitis C Virus

Wen Chen, Jyoti Dev, Julija Mezhyrova, Liqiang Pan, Alessandro Piai, and James J. Chou

Supporting Information

The unusual transmembrane partition of the hexameric channel of the Hepatitis C Virus

Wen Chen[1†], Jyoti Dev[1†], Julija Mezhyrova[2], Liqiang Pan[1], Alessandro Piai[1], James J. Chou[1,3*]

[1] Department of Biological Chemistry and Molecular Pharmacology, Harvard Medical School, Boston, Massachusetts 02115, USA.

[2] Institute of Biophysical Chemistry, Centre for Biomolecular Magnetic Resonance, J.W. Goethe-University, Frankfurt am Main, Germany

[3] State Key Laboratory of Molecular Biology, Shanghai Institute of Biochemistry and Cell Biology, Chinese Academy of Sciences, University of Chinese Academy of Sciences, Shanghai 201203, China

[†] These authors contributed equally to this work.

* Lead Contact

Correspondence should be sent to J.J.C. at james_chou@hms.harvard.edu

Table S1. Residue-specific PRE_{amp} of p7(5a) in bicelles. *Relates to Figure 3, to show the raw PREamp number and uncertainty for each of the residues.*

Figure S1. The NMR structure of the p7(5a) hexamer in DPC micelle and its presumed placement in lipid bilayer. *Relates to Figure 1, to show the overall structure of the p7(5a) hexamer determined previously in DPC micelles and the presumed transmembrane partition.*

Figure S2. TRACT measurements of p7(5a) in bicelles and in DPC micelles. *Relates to Figure 1C, to compare the dynamic properties of p7(5a) in bicelles and in DPC micelles, complementary to the secondary chemical shift comparison.*

Figure S3. OG label details. *Relates to Figure 2, to provide supporting technical details for the OG label method.*

Figure S4. Transmembrane partition of p7(5a) in bicelles. *Relates to Figure 3, to provide experimental and analysis details for the Gd-DOTA titration method for determining the protein transmembrane partition.*

Figure S5. Strips of lipid-p7(5a) and water-p7(5a) NOEs in bicelles. *Relates to Figure 4, to show the raw NOE data that report protein-lipid contacts in bicelles.*

Table S1. Residue-specific PRE_{amp} of p7(5a) in bicelles [1]. *Relates to Figure 3, to show the raw PREamp number and uncertainty for each of the residues.*

Residue	PRE_{amp}	R^2_{adj}	*Residue*	PRE_{amp}	R^2_{adj}
K3	0.935±0.014	1.000	**V32**	0.636±0.036	0.946
N4	0.892±0.027	0.982	**K33**	0.719±0.054	0.986
V5	0.865±0.018	0.990	**G34**	0.737±0.046	0.972
L6	0.874±0.024	0.982	**R35**	0.751±0.044	0.959
V7	0.871±0.026	0.980	**L36**	0.758±0.036	0.949
L8	0.862±0.027	0.976	**V37**	0.764±0.034	0.944
N9	0.879±0.022	0.985	**G39**	0.900±0.022	0.993
A10	0.883±0.020	0.988	**A40**	0.863±0.022	0.986
A11	0.875±0.023	0.986	**T41**	0.795±0.042	0.955
S12	0.891±0.022	0.986	**Y42**	0.835±0.032	0.972
A13	0.869±0.023	0.984	**L43**	0.775±0.029	0.961
A14	0.843±0.024	0.984	**S44**	0.795±0.025	0.979
G15	0.870±0.023	0.983	**L45**	0.783±0.020	0.999
N16	0.859±0.027	0.985	**G46**	0.765±0.029	0.960
H17	0.807±0.034	0.966	**V47**	0.697±0.030	0.954
G18	0.803±0.033	0.978	**W48**	0.625±0.034	0.974
F19	0.734±0.020	0.987	**L51**	0.585±0.040	0.956
F20	0.633±0.040	0.952	**L52**	0.588±0.030	0.945
W1	0.602±0.038	0.976	**V53**	0.619±0.039	0.974
G22	0.574±0.035	0.979	**R54**	0.645±0.037	0.962
L23	0.588±0.027	0.975	**L55**	0.666±0.034	0.987
L24	0.584±0.037	0.978	**L56**	0.738±0.034	0.944
V25	0.571±0.033	0.968	**R57**	0.778±0.029	0.964
V26	0.576±0.050	0.975	**H59**	0.881±0.030	0.986
L28	0.592±0.039	0.924	**R60**	0.915±0.023	0.990
A29	0.617±0.050	0.968	**A61**	0.932±0.019	0.994
W30	0.616±0.033	0.954	**L62**	0.914±0.023	0.983
H31	0.630±0.045	0.963	**A63**	0.893±0.029	0.972

[1] The results of fitting the PRE vs. [Gd-DOTA] data points to the exponential decay function (Eq. 3 in Start Methods) for each of the residues with analyzable NMR peaks to determine residue-specific PRE amplitude. R^2_{adj} is the adjusted coefficient of determination of each fitting. The bicelle *q* used for the measurements is 0.6.

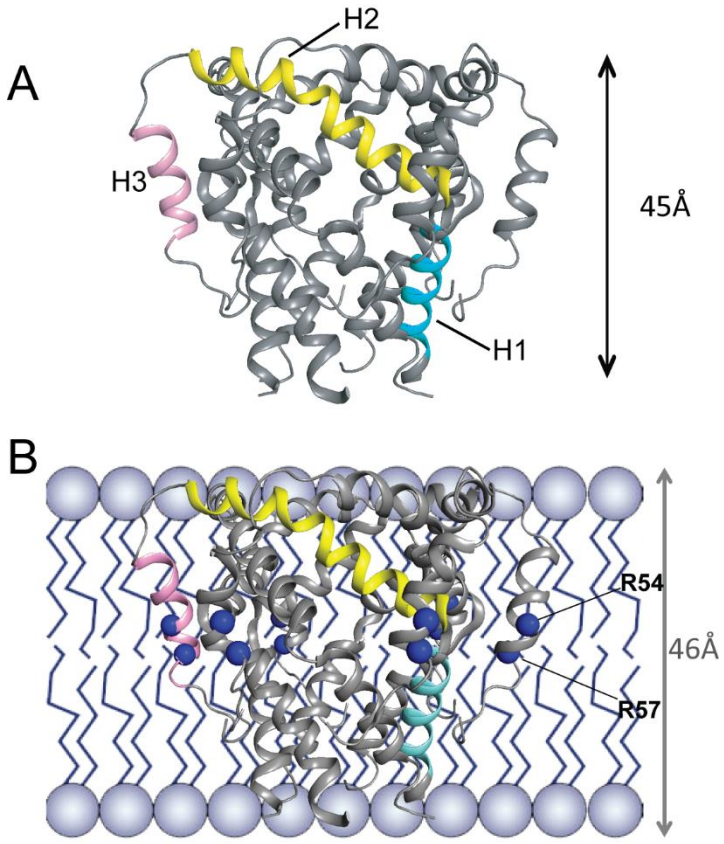

Figure S1. The NMR structure of the p7(5a) hexamer in DPC micelle and its presumed placement in lipid bilayer. *Relates to Figure 1, to show the overall structure of the p7(5a) hexamer determined previously in DPC micelles and the presumed transmembrane partition.*

(A) Ribbon representation of the p7(5a) hexamer structure solved in DPC micelles (PDB ID: 2M6X), highlighting the three transmembrane helical segments in different colors. The H1, H2 and H3 helices are shown in cyan, yellow, and pink, respectively. The hexamer structure spans about 45 Å along the symmetry axis.

(B) The presumed partition of the p7(5a) hexamer structure in an ideal lipid bilayer with ~46 Å in thickness, highlighting several basic residues, R54 and R57 (blue spheres), deep within the hydrophobic core of the lipid bilayer.

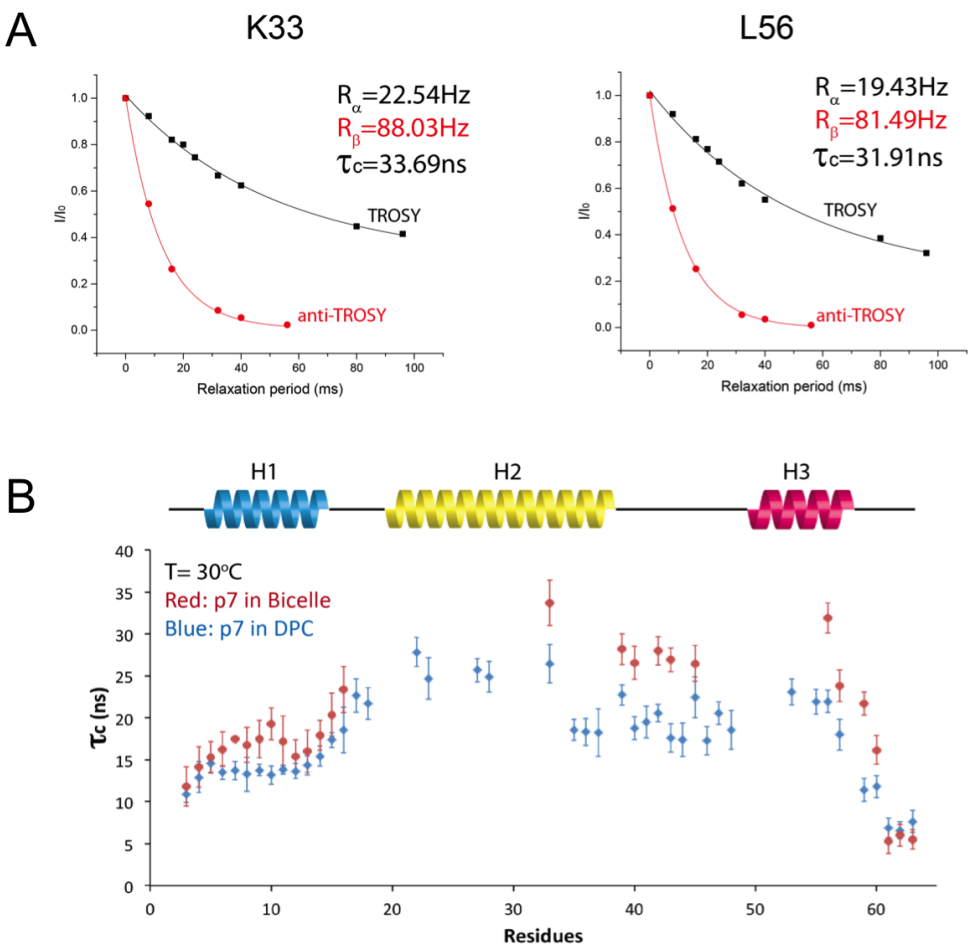

Figure S2. TRACT measurements of p7(5a) in bicelles and in DPC micelles. *Relates to Figure 1C, to compare the dynamic properties of p7(5a) in bicelles and in DPC micelles, complementary to the secondary chemical shift comparison.*

(A) TRACT measurements for residues K33 and L56 in the core of p7(5a) reconstituted in bicelles with *q* = 0.6. The protein was ^{15}N- and 85% ^{2}H- labeled. The TRACT experiment (Lee et al., 2006) was performed in 2D ^{1}H-^{15}N correlation mode to resolve resonance overlap. The plots show decay of relative peak intensity, I/I$_0$, due to ^{15}N transverse relaxation for the TROSY (black) and anti-TROSY (red) components. The TROSY relaxation rate (R$_\alpha$) and the anti-TROSY relaxation rate (R$_\beta$) were obtained by exponential fitting. τ_c was calculated using the difference R$_\beta$ - R$_\alpha$ as described in (Lee et al., 2006). The data were collected at 600 MHz and 30 °C.

(B) Comparison of residue-specific τ_c between p7(5a) in bicelles and p7(5a) in DPC micelles. The bicelle *q* used for the measurement was 0.55. The DPC sample was prepared exactly as described in (OuYang et al., 2013). In both bicelle and micelle samples, (^{15}N, 85% ^{2}H)-labeled protein was used. For the bicelle sample, most of the residues from H2 and H3 could not be analyzed due to rapid signal decay. Nevertheless, the resonances of K33 and L56 could be analyzed and yielded τ_c values (~33 ns) that are significantly larger than the corresponding values from the micelle sample (~24 ns).

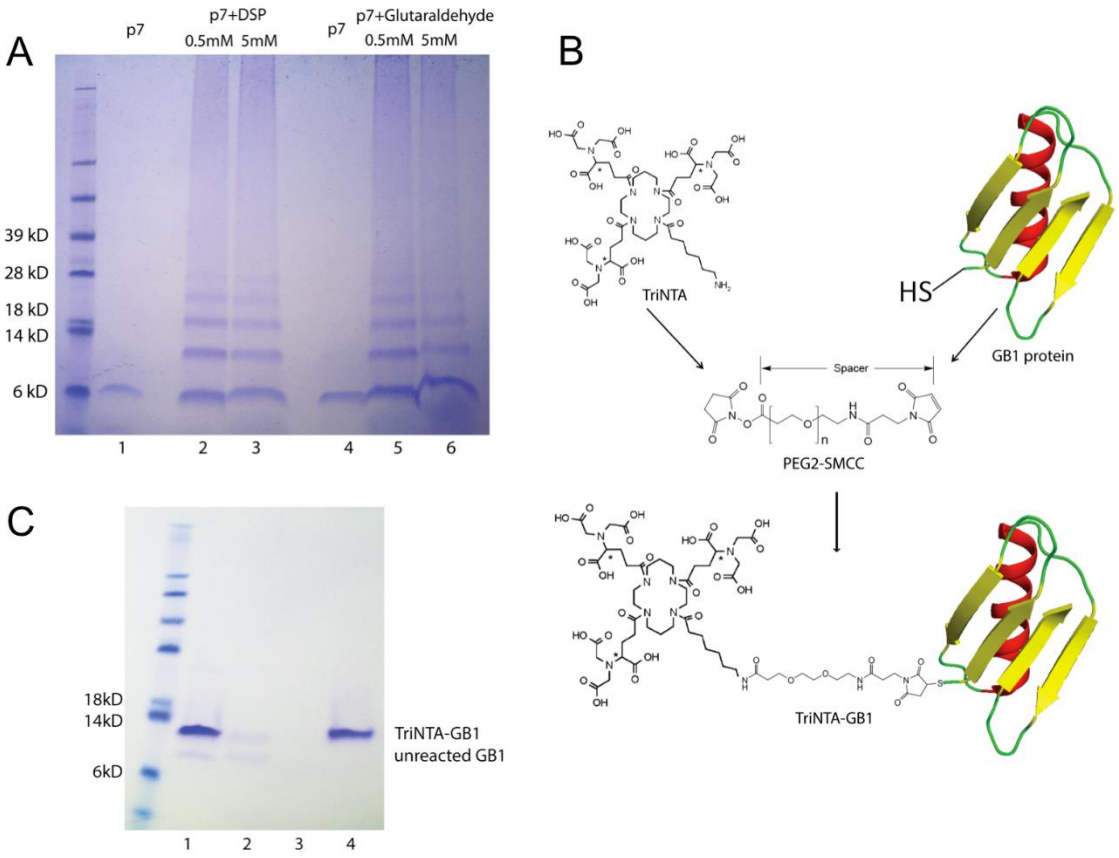

Figure S3. OG label details. *Relates to Figure 2, to provide supporting technical details for the OG label method.*

(A) Direct chemical cross-linking of bicelle-reconstituted p7(5a) with Lomant's reagents. p7(5a) was reconstituted in bicelles exactly as the NMR sample. The protein concentration was 0.05 mM. The reaction mixture contained 10 μl p7(5a) sample and various amounts of DSP (dithiobis(succinimidyl propionate)) or glutaraldehyde. DSP reactions proceeded for 30 min before quenching by 20 mM Tris (pH 7.5). Glutaraldehyde reactions proceeded for 5 min before quenching by 20 mM Tris (pH 7.5). **Lane 1, 4**: the bicelle-reconstituted p7(5a) ran as monomers in SDS-PAGE; **Lane 2, 3**: p7(5a) reacted with 10 fold (0.5 mM) and 50 fold (5 mM) molar excess of DSP cross-linker, respectively; **Lane 5, 6**: p7(5a) reacted with 10 fold (0.5 mM) and 50 fold (5 mM) molar excess of glutaraldehyde cross-linkers, respectively. All cross-linked samples showed non-specific ladders of p7(5a) and smears of aggregated cross-linking species.

(B) The reaction scheme for conjugating the primary amine of TriNTA to the free thiol group of GB1 via the bi-functional PEG2-SMCC linker. In the scheme, the NHS (*N* - hydroxysuccinimide) ester of SMCC reacts with amine group of TriNTA with extremely high efficiency (>95%). The SMCC maleimide group reacts with the GB1's thiol group. The modified sequence of GB1 is:
MGCKDKDKDKWSHPQFEKMQYKLILNGKTLKGETTTEAVDAATAEKVFKQYANDNGV
DGEWTYDDATKTFTVTE.

(C) SDS-PAGE analysis of reaction completion. Here, PEG12-SMCC, instead of PEG2-SMCC, was used to better resolve the M.W. of conjugated and unconjugated GB1s in the SDS-PAGE. TriNTA was first reacted with PEG12-SMCC. The reacted TriNTA-PEG12-SMCC, purified by HPLC, was then added to GB1 to form TriNTA-GB1 conjugate. Detailed procedure can be found in method section. **Lane 1**: maleimide reaction efficiency between TriNTA-PEG12-SMCC and GB1 is close to 90%. **Lane 2**: flow-through of the reacted solution from His_6-tag resin, showing that most GB1 is conjugated to TriNTA and thus was retained by the resin. **Lane 3**: wash of the resin to remove species that were not successfully conjugated. **Lane 4**: elution from the resin by addition of 0.2 M imidazole

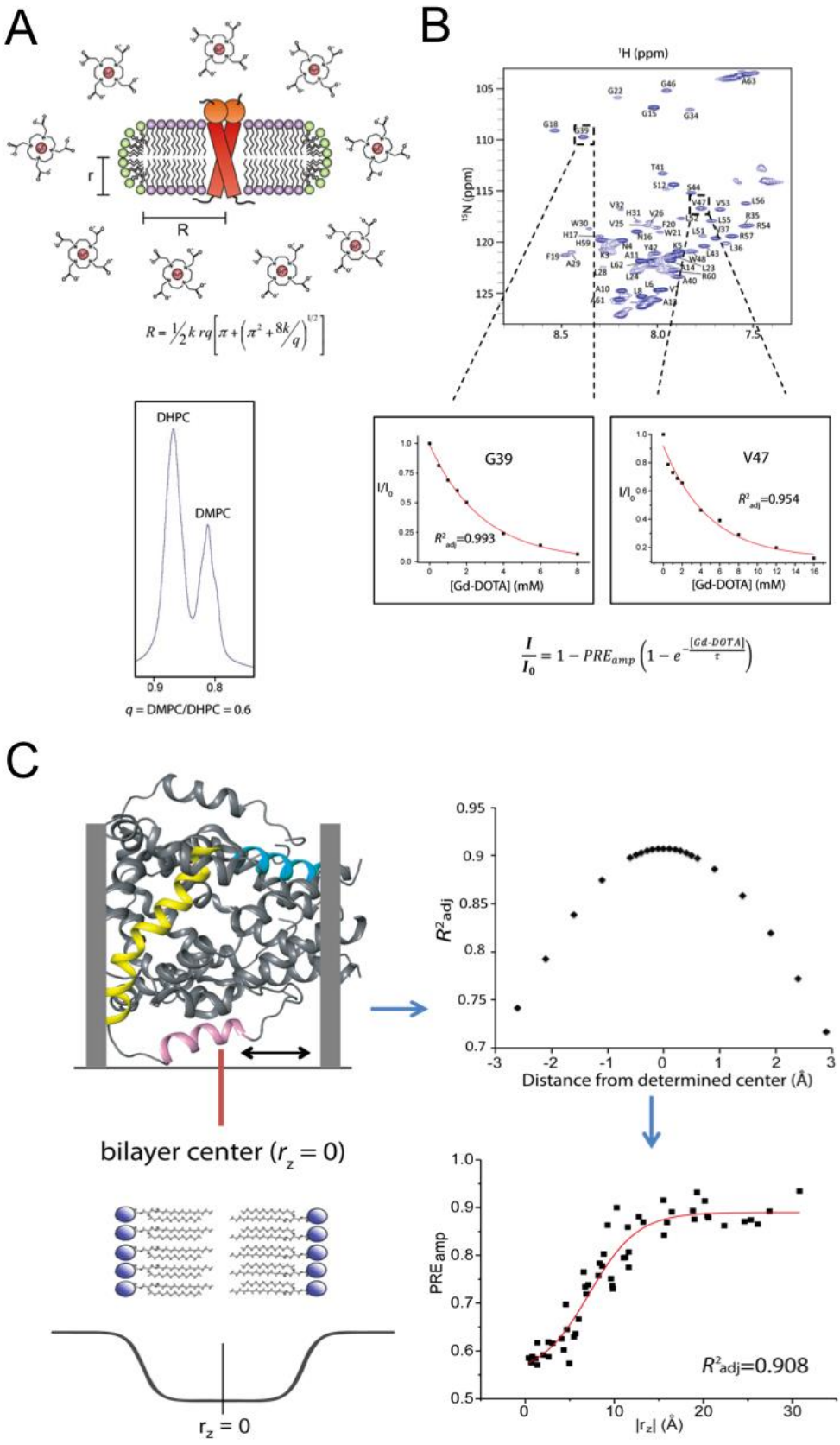
A
r
R
$R = \frac{1}{2} k\, rq\left[\pi + \left(\pi^2 + \frac{8k}{q}\right)^{1/2}\right]$
DHPC
DMPC
0.9
0.8
q = DMPC/DHPC = 0.6
B
^{1}H (ppm)
^{15}N (ppm)
8.5
8.0
7.5
G39
R^2_{adj}=0.993
I/I$_0$
[Gd-DOTA] (mM)
V47
R^2_{adj}=0.954
$\frac{I}{I_0} = 1 - PRE_{amp}\left(1 - e^{-\frac{[Gd\text{-}DOTA]}{\tau}}\right)$
C
bilayer center ($r_z = 0$)
$r_z = 0$
R^2adj
Distance from determined center (Å)
PREamp
R^2adj=0.908
|r$_z$| (Å)

Figure S4. Transmembrane partition of p7(5a) in bicelles. *Relates to Figure 3, to provide experimental and analysis details for the Gd-DOTA titration method for determining the protein transmembrane partition.*

(A) Schematic illustration of titrating the bicelle-reconstituted p7(5a) with Gd-DOTA (upper panel). The radius of the bilayer region of the bicelle (*R*) is given by the equation (Glover et al., 2001; Sanders and Schwonek, 1992) below the drawing, where *r* is the radius of the DHPC rim (20 Å), *q* is the molar ratio of DMPC to DHPC, and *k* is the ratio of the head group area of DHPC to that of DMPC. Lower panel is the 1D ^{1}H spectrum of the bicelle sample recorded at 600 MHz, showing that the peak intensity ratio of the DMPC terminal methyl groups to that of the DHPC terminal methyl groups is 0.6 (or q = 0.6).

(B) PRE vs. [Gd-DOTA] for G39 and V47, measured with a series of ^{1}H-^{15}N TROSY-HSQC spectra recorded at different Gd-DOTA concentrations. The data were fitted to the exponential decay function (Eq. 3 in Methods) to determine the PRE amplitude (PRE_{amp}). The PRE is defined as the ratio of peak intensity in the presence (I) and absence (I_0) of Gd-DOTA. The PRE_{amp} vs. residue number is shown in Fig. 3A.

(C) Assignment of the bilayer center to the p7(5a) structure by data fitting.
Left: Illustration for showing the sliding of the p7(5a) structure along the 6-fold axis (or bilayer normal) to yield best fit to the symmetric sigmoidal function (Eq. 4 in Methods). The r_z = 0 of the sigmoidal function corresponds to the bilayer center.
Right upper: The adjusted coefficient of determination (R^2_{adj}) from data fitting versus deviation from the true bilayer center. The plot shows that R^2_{adj} is a reliable indicator of the protein position with an error of about ± 0.1 Å.
Right lower: The best fit of the PRE_{amp} vs. r_z data to the symmetric sigmoidal function. The same fit is shown in Fig. 3C.

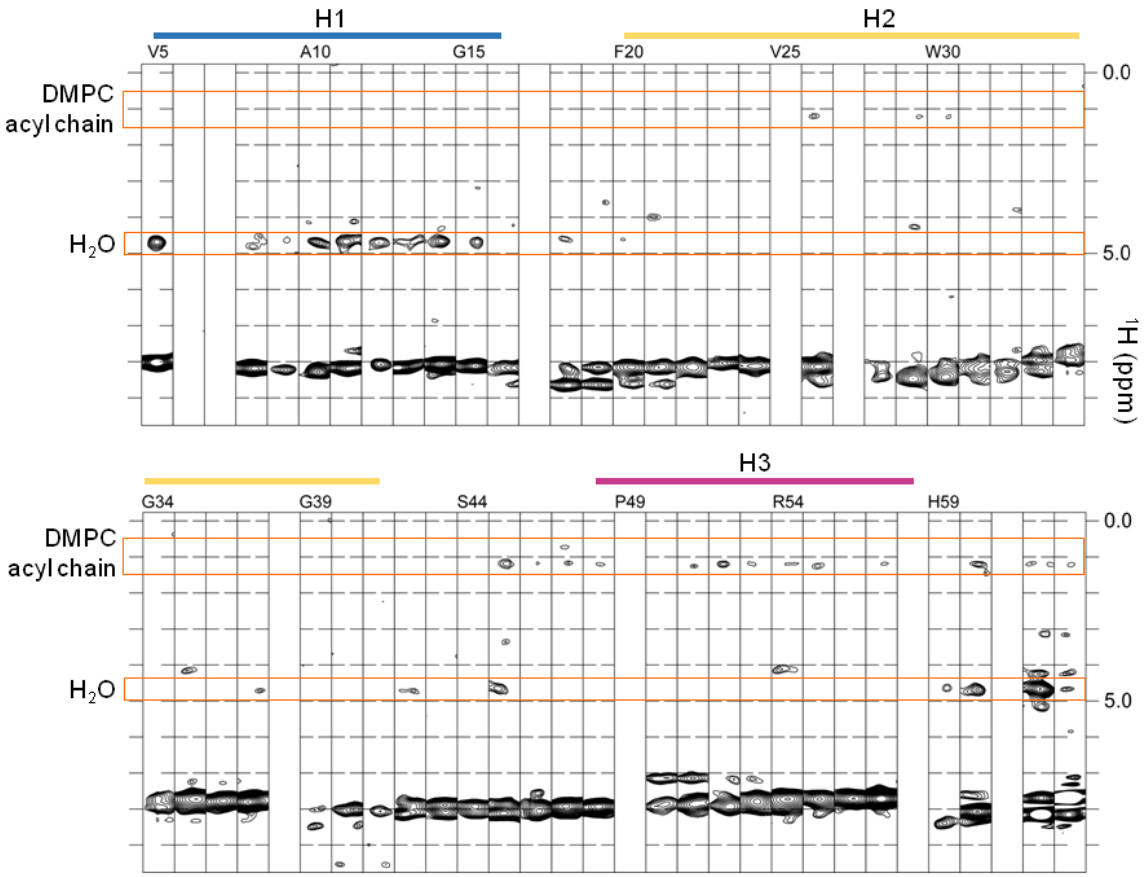

Figure S5. Strips of lipid-p7(5a) and water-p7(5a) NOEs in bicelles. *Relates to Figure 4, to show the raw NOE data that report protein-lipid contacts in bicelles.*

Strips from the 3D ^{15}N-edited NOESY-TROSY-HSQC spectrum recorded with (^{15}N, ^{2}H)-labeled p7(5a) in q = 0.6 bicelles (regular DMPC and deuterated DHPC). The NOE mixing time was set to 160 ms. Empty strips indicate prolines or residues that could not be reliably analyzed due to extremely weak resonance or spectral overlap.